

# Spectral optical monitoring of the double peaked emission line AGN Arp 102B: II. Variability of the broad line properties

L.Č. Popović<sup>1,2</sup>, A.I. Shapovalova<sup>3</sup>, D.Ilić<sup>2,4</sup>, A.N.Burenkov<sup>3</sup>, V.H. Chavushyan<sup>5</sup>, W. Kollatschny<sup>6</sup>, A. Kovačević<sup>2,4</sup>, J. R. Valdés<sup>5</sup>, J. León-Tavares<sup>5,8</sup>, N.G. Bochkarev<sup>7</sup>, V. Patiño-Álvarez<sup>5</sup>, and J. Torrealba<sup>5</sup>

<sup>1</sup> Astronomical Observatory, Volgina 7, 11160 Belgrade 74, Serbia

<sup>2</sup> Isaac Newton Institute of Chile, Yugoslavia Branch

<sup>3</sup> Special Astrophysical Observatory of the Russian AS, Nizhnij Arkhyz, Karachaevo-Cherkesia 369167, Russia

<sup>4</sup> Department of Astronomy, Faculty of Mathematics, University of Belgrade, Studentski trg 16, 11000 Belgrade, Serbia

<sup>5</sup> Instituto Nacional de Astrofísica, Óptica y Electrónica, Apartado Postal 51, CP 72000, Puebla, Pue. México

<sup>6</sup> Institut für Astrophysik, Friedrich-Hund-Platz 1, Göttingen, Germany

<sup>7</sup> Sternberg Astronomical Institute, Moscow, Russia

<sup>8</sup> Finnish Centre for Astronomy with ESO (FINCA), University of Turku, Väisäläntie 20, FI-21500 Piikkiö, Finland

Received / Accepted

## ABSTRACT

**Context.** We investigate a long-term (26 years, from 1987 to 2013) variability in the broad spectral line properties of the radio galaxy Arp 102B, an active galaxy with broad double-peaked emission lines. We use observations presented in Paper I (Shapovalova et al. 2013) in the period from 1987 to 2011, and a new set of observations performed in 2012–2013.

**Aims.** To explore the BLR geometry, and clarify some contradictions about the nature of the BLR in Arp 102B we explore variations in the H $\alpha$  and H $\beta$  line parameters during the monitored period.

**Methods.** We fit the broad lines with three broad Gaussian functions finding the positions and intensities of the blue and red peaks in H $\alpha$  and H $\beta$ . Additionally we fit averaged line profiles with the disc model.

**Results.** We find that the broad line profiles are double-peaked and have not been changed significantly in shapes, beside an additional small peak that, from time to time can be seen in the blue part of the H $\alpha$  line. The positions of the blue and red peaks have not changed significantly during the monitored period. The H $\beta$  line is broader than H $\alpha$  line in the monitored period. The disc model is able to reproduce the H $\beta$  and H $\alpha$  broad line profiles, however, observed variability in the line parameters are not in a good agreement with the emission disc hypothesis.

**Conclusions.** It seems that the BLR of Arp 102B has a disc-like geometry, but the role of an outflow can also play an important role in observed variation of the broad line properties.

**Key words.** galaxies: active – galaxies: quasar: individual (Arp 102B) – line: profiles

## 1. Introduction

Arp 102B, a LINER like object, was the first active galaxy where the broad line double-peaked profiles have been modeled with emission of an accretion disc (Chen et al., 1989; Chen & Halpern, 1989). After that, this galaxy has been widely accepted as a prototype of an AGN with broad lines emitted from the disc (see Chen & Halpern, 1989; Sulentic et al., 1990; Eracleous & Halpern, 1994; Eracleous et al., 1997) and has been studied intensively through different monitoring campaigns (see e.g. Miller & Peterson, 1990; Newman et al., 1997; Sergeev et al., 2000; Gezari et al., 2007; Shapovalova et al., 2013).

In general, the monitoring campaigns agree that the broad line region (BLR) in Arp 102B, where the double-peaked broad emission lines are forming, seems to have a disc-like geometry, but there are still some open issues and contradictions concerning the disc model (Miller & Peterson, 1990; Newman et al., 1997; Sergeev et al., 2000; Gezari et al., 2007; Shapovalova et al., 2013). The broad H $\alpha$  line profile variation,

observed by Sergeev et al. (2000) from 1992 to 1996, corresponds to gas rotating in the disc with in-homogeneity in the surface brightness, that is in an agreement with result of Gezari et al. (2007), they found that the accretion disc is the most favorable model. However, Gezari et al. (2007) concluded that the most of the observed facts fail to explain the variability of the profiles assuming processes in the accretion disc. Additional disagreement with disc model was reported by Miller & Peterson (1990), they showed that, at least at some epochs, the long-wavelength side of the line profile is higher than the short-wavelength side, contrary to what is expected from a relativistic disc, i.e. an asymmetric relativistic disc cannot explain the peak ratio observed in some periods. A sinusoidal variation of the red-to-blue peak flux ratio is present in the H $\alpha$  line profile (Newman et al., 1997; Shapovalova et al., 2013). This variation can be explained as a transient orbiting hot spot in the accretion disc<sup>1</sup>.

Additionally, it is confirmed that high ionized lines, as Ly $\alpha$  and CIV  $\lambda$ 1550 do not show the disc-like profile (two peaks) and that the Ly $\alpha$  line is single-peaked (Halpern et al., 1996), i.e. that

Send offprint requests to: A. I. Shapovalova,  
e-mail: ashap@sao.ru

<sup>1</sup> Similar variation can also be a consequence of gravitational lensing from a massive body close to primary black hole (Popović et al., 2001)

the  $\text{Ly}\alpha/\text{H}\beta$  ratio is less than 0.12 in the displaced peaks. The lack of double-peaked high ionization lines from the disc can indicate that the disc medium is too dense for those lines and that they cannot be emitted from the disc. However, it is interesting that in the near-infrared no trace of double-peaked HI lines (Riffel et al., 2006). Moreover both the Brackett and Paschen series are almost absent apart from  $\text{Pa}\alpha$  and  $\text{Pa}\beta$ .

One of the way to confirm the disc emission in the broad lines is to observe polarization in broad lines (see e.g. Corbett et al., 1998, 2000; Afanasiev et al., 2014), since the expected position angle of polarization should be parallel to the disc plane. This angle is the same as the direction of the radio jet (Antonucci et al., 1996; Corbett et al., 1998, 2000), that is not expected for the broad lines emitted from an accretion disc. Also, Chen et al. (1997) found discrepancies between the disc model and the spectropolarimetric data, but they found that if some specific conditions are taken into account, the observations could be explained with emission of the accretion disc.

Although the double-peaked broad lines of Arp 102B indicate an accretion disc emission, there are some deviations in broad line profile variations that may indicate another geometry. In Paper I (Shapovalova et al., 2013) we present observations and variation in line fluxes and the continuum. In this paper we discuss the long term spectral line profile variations in order to clarify the nature of the broad line region in Arp 102B. The paper is organized as follows: in §2 we describe our observations and used methods of analysis, in §3 we present our results of the line profile variation analysis, in §4 we discuss our results; and finally in §5 we outline our conclusions.

## 2. Observations and methods of analysis

### 2.1. Observations

Spectra of Arp 102B were taken during the monitoring period 1987–2010 with 5 different telescopes: 6 m and 1 m telescopes of the SAO RAS (Russia), two 2.1 m telescopes in Mexico (Guillermo Haro Observatory, GHO, and the Observatorio Astronomico Nacional at San Pedro Martir, OAN-SPM), and two telescopes in Spain (3.5 m and 2.2 m telescopes of Calar Alto observatory). Details of observation and data reduction are given in Paper I, and here will not be repeated.

In addition to the observational data presented in Paper I, we added 10 new spectra observed in 2012–2013 period with 2.1 m telescope of GHO. The measurements of the continuum at 5100 Å,  $\text{H}\alpha$ , and  $\text{H}\beta$  fluxes are given in Table 1. To compare new observations with ones given in Paper I, we plot in Fig. 1 the light curves in the continuum and in the broad lines. As it can be seen from Fig. 1, the minimum in the line flux is observed in 2012–2013, while the continuum flux is similar as one observed in the 1989–1992 period.

### 2.2. Method of analysis

To explore the broad line profile variability in details, we performed the following methods of analysis:

a) To subtract the narrow lines and obtain only the broad profiles, we fitted all  $\text{H}\alpha$  and  $\text{H}\beta$  lines with Gaussian functions. There is a problem to remove the narrow lines in Arp 102B, since they are right on top of the red peak in both broad lines ( $\text{H}\alpha$  and  $\text{H}\beta$ ) and the measured properties of the red peak can be strongly affected by the narrow line removal procedure. We discuss this in more details in the Appendix, and here we

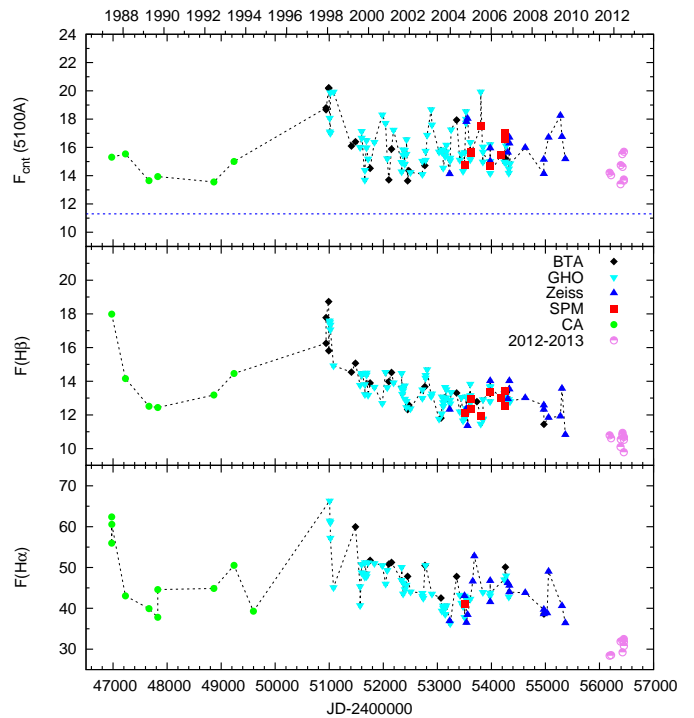


**Fig. 1.** Light-curves with the new data in the 2012–2013 period. From top to bottom: the blue continuum flux, the  $\text{H}\beta$  and  $\text{H}\alpha$  line flux. Observations with different telescopes are denoted with different symbols given in the middle plot. The continuum flux is plotted in units of  $10^{-16}\text{erg cm}^{-2}\text{s}^{-1}\text{\AA}^{-1}$ , and the line flux in units of  $10^{-14}\text{erg cm}^{-2}\text{s}^{-1}$ . The dashed line in the blue and red continuum light-curves mark the contribution of the host galaxy starlight-continuum.

**Table 1.** Measurements of line fluxes of the new set of observations in the 2012–2013 period. The continuum flux is in units of  $10^{-16}\text{erg cm}^{-2}\text{s}^{-1}\text{\AA}^{-1}$ , and the line flux in units of  $10^{-14}\text{erg cm}^{-2}\text{s}^{-1}$ .

N	UT-date	MJD	$F_{\text{cnt}}5100\text{\AA}$	$F(\text{H}\beta)$	$F(\text{H}\alpha)$
1	2012Sep17	56187.69	14.21	10.78	28.40
2	2012Oct14	56214.67	14.03	10.61	28.53
3	2013Apr07	56389.99	13.39	10.10	31.88
4	2013Apr11	56393.98	14.74	10.55	-
5	2013May10	56422.87	15.52	10.82	32.07
6	2013May13	56425.82	14.63	10.94	-
7	2013May14	56426.81	-	-	29.22
8	2013Jun06	56449.86	13.65	10.52	32.49
9	2013Jun07	56450.87	15.69	10.69	31.76
10	2013Jun08	56451.87	13.73	9.78	30.76

shortly describe the subtraction procedure. To estimate the narrow line contribution we fitted simultaneously the whole  $\text{H}\alpha$  and  $\text{H}\beta$  profiles (broad + narrow lines). We used three broad Gaussian functions for the broad component of the  $\text{H}\alpha$  and  $\text{H}\beta$  lines (Fig. 2), while for all narrow lines we assumed the same widths and shifts (see Popović et al., 2004). We assumed that the ratio of  $[\text{OIII}]4959$  and  $[\text{OIII}]5007$  follows the flux ratio 1:3 (Dimitrijević et al., 2007), and the same for  $[\text{NII}]$  doublet:  $F[\text{NII}]6584/F[\text{NII}]6548 \sim 3$ . In the  $\text{H}\alpha$  wavelength band, the  $[\text{SII}]6717,6731$  doublet, and  $[\text{OI}]6300$  and  $[\text{OI}]6363$  lines were fitted using single Gaussian. Note here that only one Gaussian

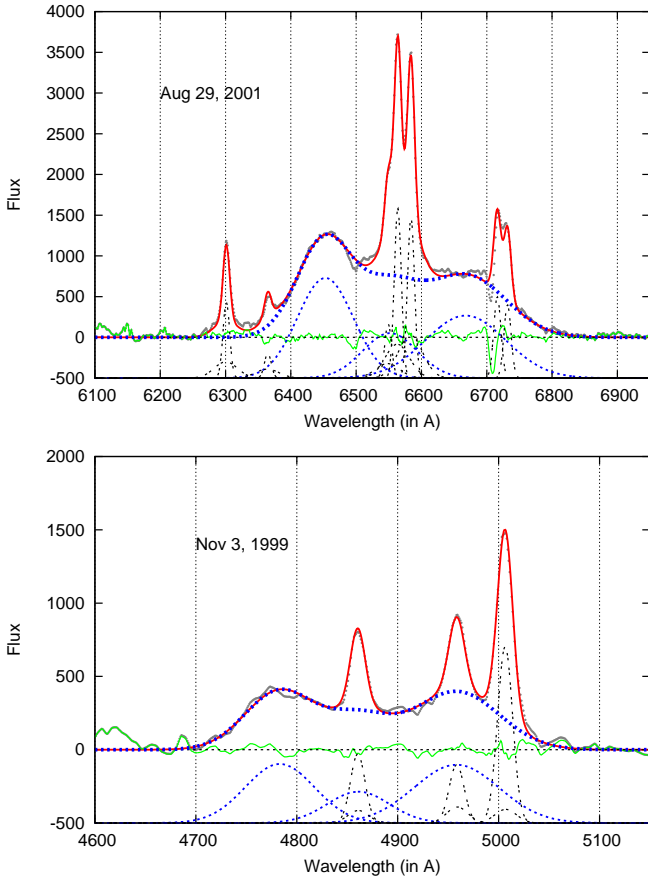


**Fig. 2.** Examples of the best Gaussian fit of one epoch  $H\alpha$  (upper panel) and  $H\beta$  line (bottom panel). Below the observed spectrum (dots), model (solid line), and residual (thin solid line), the Gaussian components are given, where broad components are denoted with dashed line and narrow components with double-dashed line. The thick dashed line reproduce the modeled broad component of the fitted Balmer line.

cannot properly fit the narrow line wings, therefore we included an additional, broader, Gaussian (with significantly smaller intensity) for fitting the narrow line wings. As it can be seen in Fig. 2, the three broad components (red and blue shifted, and a central one) can satisfactorily explain the broad line profiles. To check the narrow line subtraction we perform several tests, see Appendix for details.

b) After subtraction of the narrow lines and continuum, we made month-averaged line profiles using similar profiles (same peak positions and total line flux differs up to  $\sim 10\%$ ). These month-averaged line profiles are given for both  $H\alpha$  and  $H\beta$  line in Figs. 3 and 4, and we further continued to measure and analyze properties of these profiles.

c) To determine the peak positions in the  $H\alpha$  and  $H\beta$  broad line profiles, we performed again the Gaussian analysis, but now of the month-averaged broad profile. The broad profile was fitted with three Gaussian functions, corresponding to the blue, central, and red component (Fig. 5). By the inspection of the parameters obtained from the Gaussian fittings, we note that the central component is very often changing the position, and affects other parameters, especially the intensity of the red peak. Therefore, additionally we fitted the month-averaged broad line profiles using the constraint that the central component should not be with large shift velocity, i.e. putting the limits to the shift

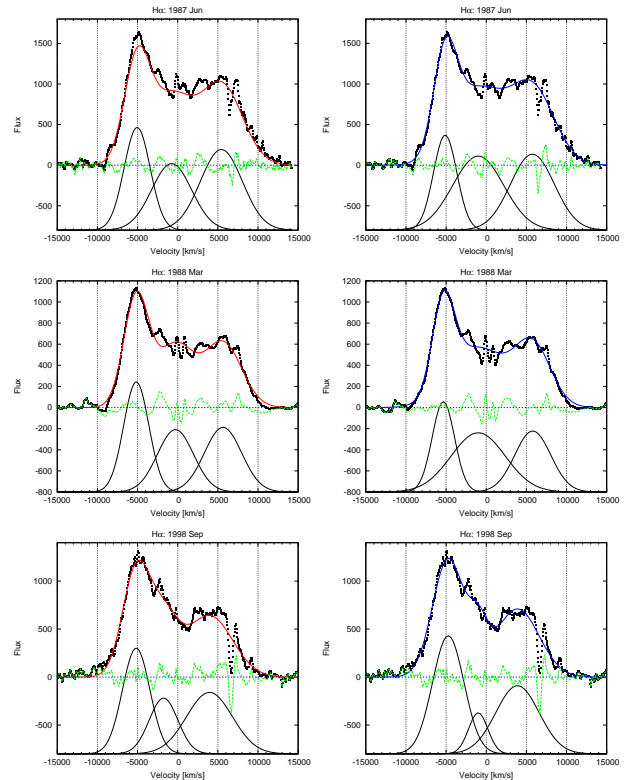


**Fig. 5.** Month-averaged  $H\alpha$  broad component fitted with Gaussians using two different assumptions: all parameters are free (left panels) and the shift of the central component is limited (right panels). Below the observed spectrum (dots), model (solid line), and residual (dashed line), the three broad Gaussian components are given. Each plot is labeled with the observed month and year.

of the central component between  $-1000 \text{ km s}^{-1}$  and  $600 \text{ km s}^{-1}$  (see Figs. 5 and 6, and the discussion in Appendix). The obtained error-bars of the parameters from both fittings are often smaller than the difference between the parameters obtained from these two fitting procedures, therefore we accepted for the line parameters the averaged value of the two best-fittings, while for their error-bars we took the corresponding standard deviation, i.e. the discrepancy between the averaged parameters and ones obtained from the fits. The averaged parameters with their uncertainties of the Gaussian fittings of the broad  $H\alpha$  and  $H\beta$  components are given in Tables 2 and 3.

d) The broad double-peaked line profiles are usually fitted with some sort of disc model (see e.g. Eracleous & Halpern, 1994; Gezari et al., 2007; Newman et al., 1997; Popović et al., 2011, etc.). Here we use a relativistic disc model given by Chen et al. (1989) and Chen & Halpern (1989) to model the broad  $H\alpha$  profile. In Fig. 7 we present disc fitting with our parameters and ones given in Gezari et al. (2007), we will discuss this in more details in §3.2.

e) Finally, we measured the Full Width at Half Maximum (FWHM) and Full Width at Quarter (1/4) Maximum (FWQM). These measurements are also given in Tables 2 and 3.

### 3. The broad line profile variability

In Paper I we measured and analyzed variations in the continuum and line fluxes using total of 118 spectra covering the  $H\beta$  wavelength region, and 90 spectra covering the  $H\alpha$  line. We showed

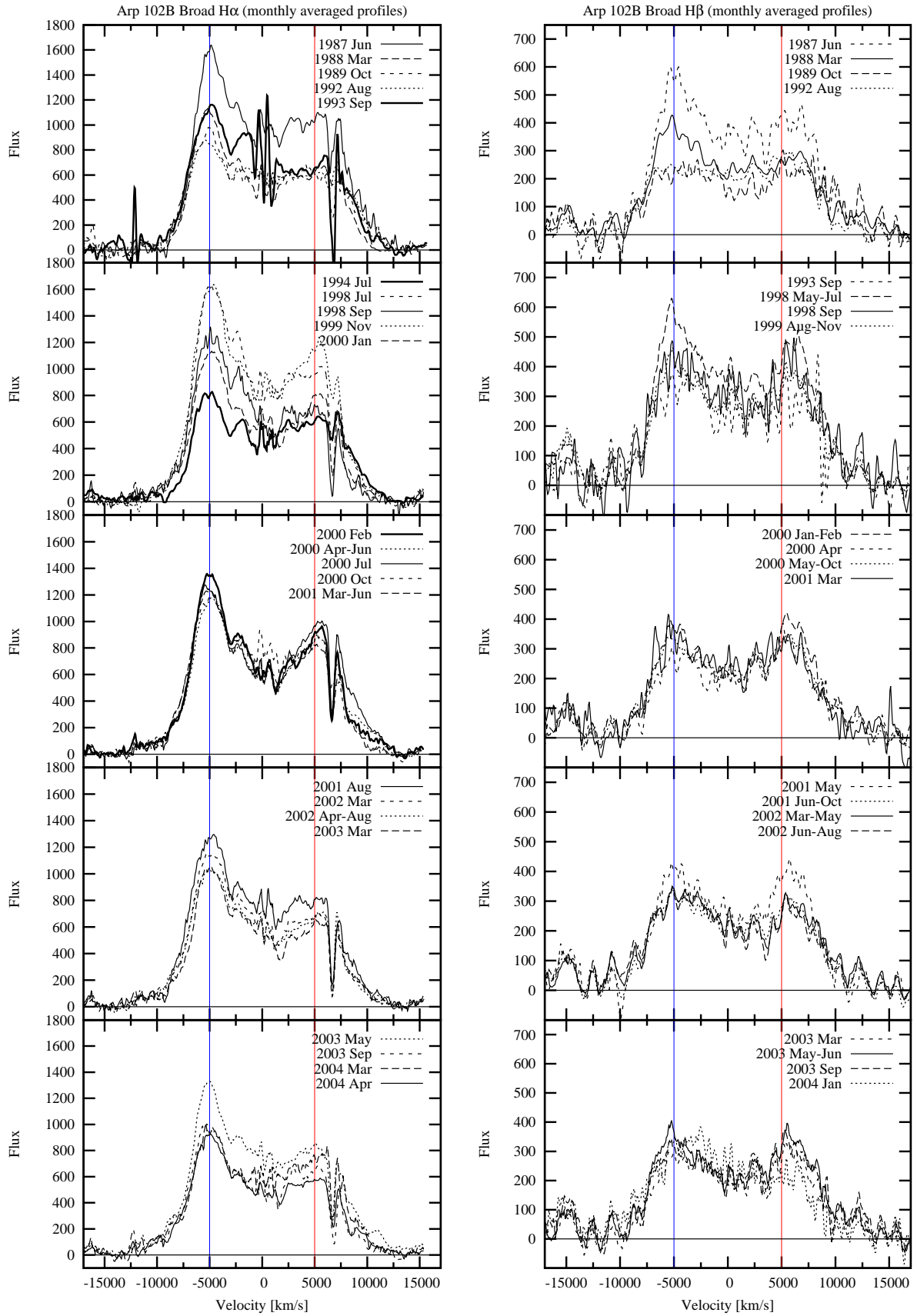


**Fig. 3.** Month-averaged profiles of the H $\alpha$  and H $\beta$  broad emission lines in the period 1987–2004. The abscissa (OX) shows radial velocities with respect to the narrow component of the H $\alpha$  or H $\beta$  line. The ordinate (OY) shows the flux in units of  $10^{-16}\text{erg cm}^{-2}\text{s}^{-1}\text{\AA}^{-1}$ .

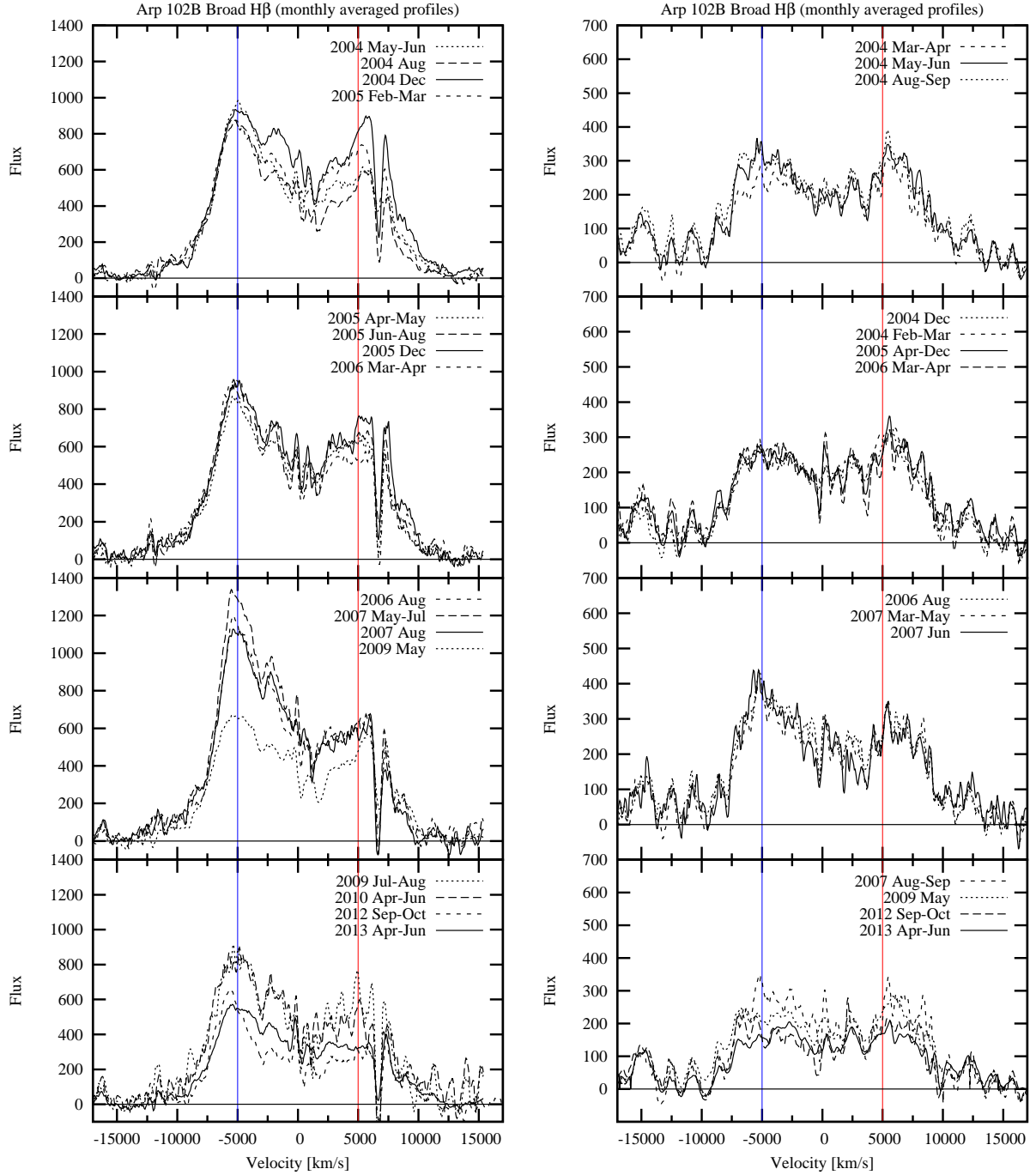


**Fig. 4.** The same as in Fig. 3, but for period 2004–2013

that the fluxes in the  $H\alpha$  and  $H\beta$  lines, and in continuum were not strongly varying (around 20% in line and  $\sim 30\%$  in continuum), and that several flare-like events were observed during the monitored period (1987–2010). Considering spectra from new observations, it seems that there is a minimum in the line emission in the 2012–2013 period (see Fig. 1), and also it can be seen in Fig. 4 that both lines are weak, moreover,  $H\beta$  is very weak with two weak peaks comparable to noise.

During the monitored period, the broad  $H\alpha$  and  $H\beta$  lines have double-peaked profiles (even in the minimum), but, as it can be seen in Figs. 3 and 4, their line shapes and widths are different. Comparing the month-averaged spectra of the  $H\alpha$  and  $H\beta$  broad lines (see Figs. 3 and 4), one can note, that there is a dif-

ference between the peak ratio of  $H\alpha$  and  $H\beta$  lines. The  $H\alpha$  line mostly has stronger blue peak, while very often the  $H\beta$  line has almost the same intensities of the blue and red peak. On the other side, the  $H\beta$  FWHM and FWQM ( $FWHM_{\text{mean}}=16100\pm 700$  km s $^{-1}$ ,  $FWQM_{\text{mean}}=17900\pm 700$  km s $^{-1}$ ) are significantly broader than the  $H\alpha$  ones ( $FWHM_{\text{mean}}=14400\pm 400$  km s $^{-1}$ ,  $FWQM_{\text{mean}}=16600\pm 800$  km s $^{-1}$ ). This is in a contradiction with the disc model predictions, i.e. if  $H\beta$  is originating closer to the central black hole (as indicated by larger line widths), it is expected that it has a more pronounced blue peak than  $H\alpha$ .

On average, the line profiles of the  $H\alpha$  and  $H\beta$  lines are not changing significantly, beside some flare-like variations seen in short periods (as e.g. in the period 1987–1992, 1998, and 2012–

**Table 2.** Parameters of the Gaussian analysis of the broad H $\alpha$  line profiles: shifts, intensities (given in  $10^{-16}$  erg cm $^{-2}$ s $^{-1}$ Å $^{-1}$ ), width of the blue, central, and red Gaussian, respectively. Measurements of the FWHM and FWQM of are also given

Year	Month	shift			intensity			width			FWHM	FWQM
		blue km s $^{-1}$	central km s $^{-1}$	red km s $^{-1}$	blue	central	red	blue km s $^{-1}$	central km s $^{-1}$	red km s $^{-1}$		
1987	Jun	-5083 ± 45	-877 ± 170	5595 ± 222	1217 ± 65	866 ± 66	964 ± 40	2180 ± 169	4005 ± 678	3784 ± 115	14300 ± 858	16700 ± 1002
1988	Mar	-5250 ± 131	-638 ± 512	5720 ± 106	949 ± 131	576 ± 21	595 ± 24	2095 ± 175	3978 ± 1132	3224 ± 74	14500 ± 870	16100 ± 966
1989	Oct	-5400 ± 4	-793 ± 293	4983 ± 447	893 ± 9	424 ± 58	611 ± 18	2552 ± 21	2714 ± 354	4800 ± 336	15300 ± 918	18100 ± 1086
1992	Aug	-5562 ± 140	-475 ± 289	6392 ± 319	701 ± 127	607 ± 18	560 ± 63	2200 ± 306	4385 ± 1216	3617 ± 185	15800 ± 948	18100 ± 1086
1993	Sep	-5208 ± 54	-785 ± 305	5263 ± 859	1070 ± 28	710 ± 72	679 ± 30	2440 ± 59	2770 ± 682	4105 ± 853	15000 ± 900	17200 ± 1032
1994	Sep	-5241 ± 91	-721 ± 395	6019 ± 182	658 ± 147	487 ± 12	576 ± 76	1937 ± 288	4401 ± 1603	3641 ± 79	14000 ± 840	17000 ± 1020
1998	Jul	-4993 ± 58	-1239 ± 338	4847 ± 642	1317 ± 230	817 ± 52	876 ± 120	2246 ± 44	3847 ± 1502	3631 ± 526	14100 ± 846	15500 ± 930
1998	Sep	-4949 ± 311	-1381 ± 539	3925 ± 49	1165 ± 92	504 ± 108	675 ± 49	2594 ± 243	2116 ± 581	3925 ± 161	14300 ± 858	15300 ± 918
1999	Nov	-4981 ± 194	-453 ± 770	5281 ± 337	1363 ± 336	758 ± 152	995 ± 78	2344 ± 366	4163 ± 1783	2957 ± 163	14600 ± 876	15800 ± 948
2000	Jan	-5040 ± 30	-682 ± 450	5293 ± 460	896 ± 233	559 ± 40	632 ± 167	2163 ± 413	4805 ± 2733	2430 ± 146	13800 ± 828	15300 ± 918
2000	Feb	-5075 ± 109	-636 ± 515	5214 ± 682	1244 ± 79	592 ± 40	813 ± 51	2374 ± 88	3084 ± 1273	3293 ± 646	14100 ± 846	15600 ± 936
2000	Apr-Jun	-5001 ± 188	-842 ± 56	5059 ± 491	1061 ± 99	485 ± 95	787 ± 35	2598 ± 109	2820 ± 1193	3802 ± 485	14300 ± 858	16400 ± 984
2000	Jul	-5095 ± 113	-1037 ± 52	5193 ± 267	1198 ± 46	507 ± 60	944 ± 39	2413 ± 80	2437 ± 543	4013 ± 350	14600 ± 876	17400 ± 1044
2000	Oct	-5122 ± 312	-694 ± 433	5150 ± 544	930 ± 337	602 ± 248	675 ± 205	2406 ± 630	4316 ± 2856	3070 ± 611	14000 ± 840	16700 ± 1002
2001	Mar-Jun	-5127 ± 74	-884 ± 165	4929 ± 333	1147 ± 33	644 ± 37	776 ± 10	2558 ± 43	2817 ± 556	3299 ± 354	14200 ± 852	16500 ± 990
2001	Aug	-5135 ± 119	-957 ± 59	4459 ± 490	1214 ± 47	546 ± 117	788 ± 21	2613 ± 75	2514 ± 633	4254 ± 445	14300 ± 858	17000 ± 1020
2002	Mar	-5058 ± 336	-959 ± 121	4779 ± 873	1041 ± 121	511 ± 192	661 ± 15	2636 ± 341	2742 ± 1405	3684 ± 784	14200 ± 852	16100 ± 966
2002	Apr-Aug	-5027 ± 288	-666 ± 172	5008 ± 465	951 ± 76	466 ± 116	653 ± 10	2906 ± 230	2673 ± 955	3613 ± 463	14400 ± 864	16900 ± 1014
2003	Mar	-5097 ± 238	-1160 ± 308	5034 ± 370	978 ± 55	537 ± 87	592 ± 5	2311 ± 258	2496 ± 689	3831 ± 420	14000 ± 840	16100 ± 966
2003	May	-5129 ± 124	-800 ± 283	4717 ± 833	1210 ± 13	564 ± 193	786 ± 8	2444 ± 243	2553 ± 968	4425 ± 1043	14100 ± 846	16800 ± 1008
2003	Sep	-5130 ± 126	-684 ± 446	4708 ± 979	930 ± 40	621 ± 148	640 ± 16	2534 ± 365	932 ± 4016	3374 ± 2020	14300 ± 858	16600 ± 996
2004	Mar	-5185 ± 66	-865 ± 192	5568 ± 292	698 ± 184	533 ± 67	593 ± 150	2027 ± 406	5318 ± 2233	3494 ± 363	14600 ± 876	17600 ± 1056
2004	Apr	-5085 ± 132	-816 ± 251	4818 ± 824	857 ± 26	349 ± 123	542 ± 40	2551 ± 343	2851 ± 1284	4043 ± 652	14400 ± 864	16500 ± 990
2004	May-Jun	-5015 ± 232	-774 ± 464	5143 ± 315	860 ± 100	374 ± 80	538 ± 33	2637 ± 206	3181 ± 1081	3970 ± 217	14100 ± 846	16400 ± 984
2004	Aug	-5070 ± 194	-649 ± 76	5269 ± 605	811 ± 41	411 ± 53	528 ± 17	2798 ± 208	2553 ± 1049	3132 ± 566	14600 ± 876	16500 ± 990
2004	Dec	-4995 ± 93	-788 ± 300	5321 ± 531	860 ± 61	519 ± 21	775 ± 6	2837 ± 12	2717 ± 1004	3686 ± 634	14800 ± 888	18000 ± 1080
2005	Feb-Mar	-5150 ± 124	-631 ± 522	4893 ± 482	802 ± 39	375 ± 42	654 ± 60	3007 ± 76	2907 ± 1185	3490 ± 501	14600 ± 876	16900 ± 1014
2005	Apr	-5151 ± 219	-774 ± 246	4757 ± 692	797 ± 4	395 ± 121	611 ± 15	2552 ± 641	2664 ± 1108	3482 ± 685	14500 ± 870	17000 ± 1020
2005	Jun-Aug	-5237 ± 240	-927 ± 104	4887 ± 521	838 ± 34	389 ± 113	645 ± 19	2707 ± 423	2738 ± 1072	3485 ± 515	14700 ± 882	16900 ± 1014
2005	Dec	-5128 ± 270	-1044 ± 62	4884 ± 294	855 ± 53	420 ± 85	690 ± 5	2804 ± 162	2369 ± 762	3990 ± 317	14800 ± 888	17800 ± 1068
2006	Mar-Apr	-5065 ± 257	-800 ± 283	4710 ± 759	923 ± 41	351 ± 210	524 ± 13	2826 ± 609	2078 ± 878	4129 ± 751	14500 ± 870	17000 ± 1020
2006	Aug	-5039 ± 273	-1106 ± 149	4655 ± 752	1056 ± 90	496 ± 156	594 ± 17	2442 ± 283	2585 ± 1007	3684 ± 584	13700 ± 822	15200 ± 912
2007	May-Jul	-5164 ± 391	-1414 ± 585	4688 ± 587	1133 ± 172	652 ± 172	605 ± 2	2389 ± 402	2583 ± 1024	3590 ± 397	13400 ± 804	15300 ± 918
2007	Aug	-5163 ± 327	-1202 ± 286	4643 ± 646	1019 ± 67	624 ± 146	596 ± 8	2405 ± 437	2497 ± 704	3256 ± 370	13900 ± 834	15700 ± 942
2009	May	-5265 ± 223	-981 ± 21	5420 ± 401	629 ± 55	278 ± 11	390 ± 15	2718 ± 117	2632 ± 933	3411 ± 589	14900 ± 894	17700 ± 1062
2009	Jul-Aug	-5249 ± 528	-1326 ± 461	4753 ± 511	769 ± 65	376 ± 170	568 ± 11	2927 ± 616	2167 ± 1179	3654 ± 314	14900 ± 894	16400 ± 984
2010	Apr-Jun	-5363 ± 211	-1190 ± 268	3724 ± 1983	704 ± 63	335 ± 255	478 ± 62	2602 ± 165	2106 ± 1256	5717 ± 3209	14700 ± 882	16700 ± 1002
2012	Sep-Oct	-5581 ± 135	-1173 ± 244	5274 ± 477	612 ± 4	274 ± 40	283 ± 24	1981 ± 249	2384 ± 415	3893 ± 630	14700 ± 882	16500 ± 990
2013	Apr-Jun	-5056 ± 86	-792 ± 295	4676 ± 993	537 ± 6	241 ± 91	333 ± 4	2823 ± 66	2365 ± 675	4499 ± 877	14800 ± 888	16800 ± 1008
mean		-5148 ± 143	-887 ± 240	5016 ± 486	946 ± 208	504 ± 141	649 ± 150	2502 ± 269	2955 ± 880	3728 ± 553	14431 ± 448	16618 ± 790

**Table 3.** The same as in Table 2, but for the broad H $\beta$  line.

Year	Month	shift			intensity			width			FWHM	FWQM
		blue km s $^{-1}$	central km s $^{-1}$	red km s $^{-1}$	blue	central	red	blue km s $^{-1}$	central km s $^{-1}$	red km s $^{-1}$		
1987	Jun	-4930 ± 326	-440 ± 791	5747 ± 434	478 ± 112	257 ± 76	377 ± 34	2640 ± 378	3907 ± 1692	3889 ± 360	15300 ± 918	17500 ± 1050
1988	Mar	-5206 ± 110	-575 ± 601	6442 ± 583	320 ± 109	221 ± 9	235 ± 63	2445 ± 282	4831 ± 2834	3964 ± 154	15500 ± 930	17100 ± 1026
1989	Oct	-4974 ± 47	-515 ± 687	6035 ± 54	231 ± 4	111 ± 10	225 ± 7	3446 ± 202	2486 ± 745	4913 ± 1017	17800 ± 1068	18900 ± 1134
1992	Aug	-5714 ± 496	-847 ± 216	5263 ± 189	215 ± 35	157 ± 27	236 ± 59	2961 ± 459	3752 ± 1299	4050 ± 21	16100 ± 966	18800 ± 1128
1993	Sep	-4968 ± 161	378 ± 315	6499 ± 1118	279 ± 119	184 ± 57	223 ± 89	3248 ± 78	5688 ± 4228	3354 ± 1184	17100 ± 1026	18900 ± 1134
1998	May-Jul	-5217 ± 156	-332 ± 945	6533 ± 48	444 ± 107	380 ± 16	416 ± 27	2184 ± 447	4848 ± 1200	2911 ± 34	15400 ± 924	17100 ± 1026
1998	Sep	-5053 ± 454	-470 ± 738	5969 ± 15	406 ± 42	273 ± 25	374 ± 8	2932 ± 394	2669 ± 803	4043 ± 62	16200 ± 972	18400 ± 1104
1999	Aug-Nov	-5052 ± 456	-419 ± 809	5998 ± 27	391 ± 20	269 ± 32	372 ± 6	3009 ± 502	2777 ± 650	4010 ± 109	15600 ± 936	17100 ± 1026
2000	Jan-Feb	-4955 ± 226	-355 ± 913	6172 ± 233	285 ± 93	194 ± 33	329 ± 53	2554 ± 695	5034 ± 3103	3250 ± 326	15400 ± 924	17600 ± 1056
2000	Apr	-4928 ± 96	-311 ± 972	5608 ± 559	264 ± 5	139 ± 38	294 ± 3	2827 ± 59	3012 ± 518	4150 ± 782	15800 ± 948	17900 ± 1074
2000	May-Oct	-5249 ± 8	265 ± 474	6161 ± 180	243 ± 71	206 ± 27	241 ± 84	2547 ± 485	6032 ± 3201	3206 ± 770	16100 ± 966	18800 ± 1128
2001	Mar	-5152 ± 210	-475 ± 743	5274 ± 317	332 ± 1	183 ± 5	320 ± 7	2963 ± 266	2753 ± 303	3889 ± 332	15700 ± 942	17400 ± 1044
2001	May	-5018 ± 162	-343 ± 928	6086 ± 124	300 ± 107	248 ± 24	358 ± 46	2583 ± 544	4989 ± 2205	2742 ± 168	14900 ± 894	17900 ± 1074
2001	Jun-Oct	-5137 ± 394	-448 ± 781	6167 ± 441	239 ± 98	192 ± 52	243 ± 45	2811 ± 743	4792 ± 2630	3482 ± 523	15700 ± 942	18200 ± 1092
2002	Mar-May	-4802 ± 125	-372 ± 796	6385 ± 37	276 ± 39	133 ± 3	263 ± 5	4032 ± 161	3875 ± 829	4064 ± 95	16100 ± 966	18400 ± 1104
2002	Jun-Aug	-4465 ± 470	-350 ± 919	6196 ± 142	314 ± 8	83 ± 66	260 ± 14	4506 ± 861	1921 ± 1100	3700 ± 187	16100 ± 966	18900 ± 1134
2003	Mar	-4987 ± 486	-438 ± 795	6071 ± 45	239 ± 35	176 ± 40	281 ± 3	2904 ± 426	3586 ± 340	3415 ± 67	15500 ± 930	17400 ± 1044
2003	May-Jun	-5163 ± 253	-469 ± 752	5980 ± 178	335 ± 12	174 ± 15	325 ± 3	2882 ± 235	3205 ± 46	3926 ± 206	15800 ± 948	17300 ± 1038
2003	Sep	-5101 ± 1	-539 ± 653	6556 ± 489	284 ± 15	118 ± 21	287 ± 13	3233 ± 129	3235 ± 1161	4846 ± 486	16400 ± 984	17900 ± 1074
2004	Jan	-4184 ± 462	304 ± 412	5807 ± 145	309 ± 19	120 ± 75	197 ± 27	4465 ± 1227	4100 ± 1563	3582 ± 22	15000 ± 900	18200 ± 1092
2004	Mar-Apr	-4713 ± 418	359 ± 342	5726 ± 168	243 ± 8	119 ± 55	254 ± 7	3925 ± 468	2491 ± 713	4019 ± 600	15800 ± 948	18600 ± 1116
2004	May-Jun	-4858 ± 110	-130 ± 1230	6447 ± 158	249 ± 99	155 ± 39	253 ± 60	3027 ± 802	6152 ± 4465	3212 ± 507	16300 ± 978	18700 ± 1122
2004	Aug-Sep	-5293 ± 28	-394 ± 851	5831 ± 223	304 ± 20	122 ± 54	300 ± 19	3762 ± 410	3256 ± 366	4010 ± 834	16400 ± 984	18200 ± 1092
2004	Dec	-5308 ± 506	-346 ± 926	6031 ± 177	214 ± 66	169 ± 24	263 ± 24	3107 ± 379	4154 ± 1635	3449 ± 2	16600 ± 996	17800 ± 1068
2005	Feb-Mar	-5032 ± 301	446 ± 9	5889 ± 134	193 ± 96	175 ± 33	227 ± 75	2926 ± 509	5799 ± 3966	2813 ± 901	15300 ± 918	18000 ± 1080
2005	Apr-Dec	-5084 ± 270	-516 ± 685	6247 ± 151	181 ± 106	169 ± 13	224 ± 71	2936 ± 431	6546 ± 4992	3427 ± 593	17200 ± 1032	18100 ± 1086
2006	Mar-Apr	-4921 ± 15	-172 ± 1169	6495 ± 64	190 ± 106	168 ± 23	200 ± 67	2956 ± 908	6612 ± 5120	3071 ± 753	16400 ± 984	17700 ± 1062
2006	Aug	-4630 ± 134	505 ± 134	6096 ± 71	356 ± 12	146 ± 7	277 ± 0	3893 ± 2	2665 ± 453	3691 ± 150	16400 ± 984	17600 ± 1002
2007	May	-										

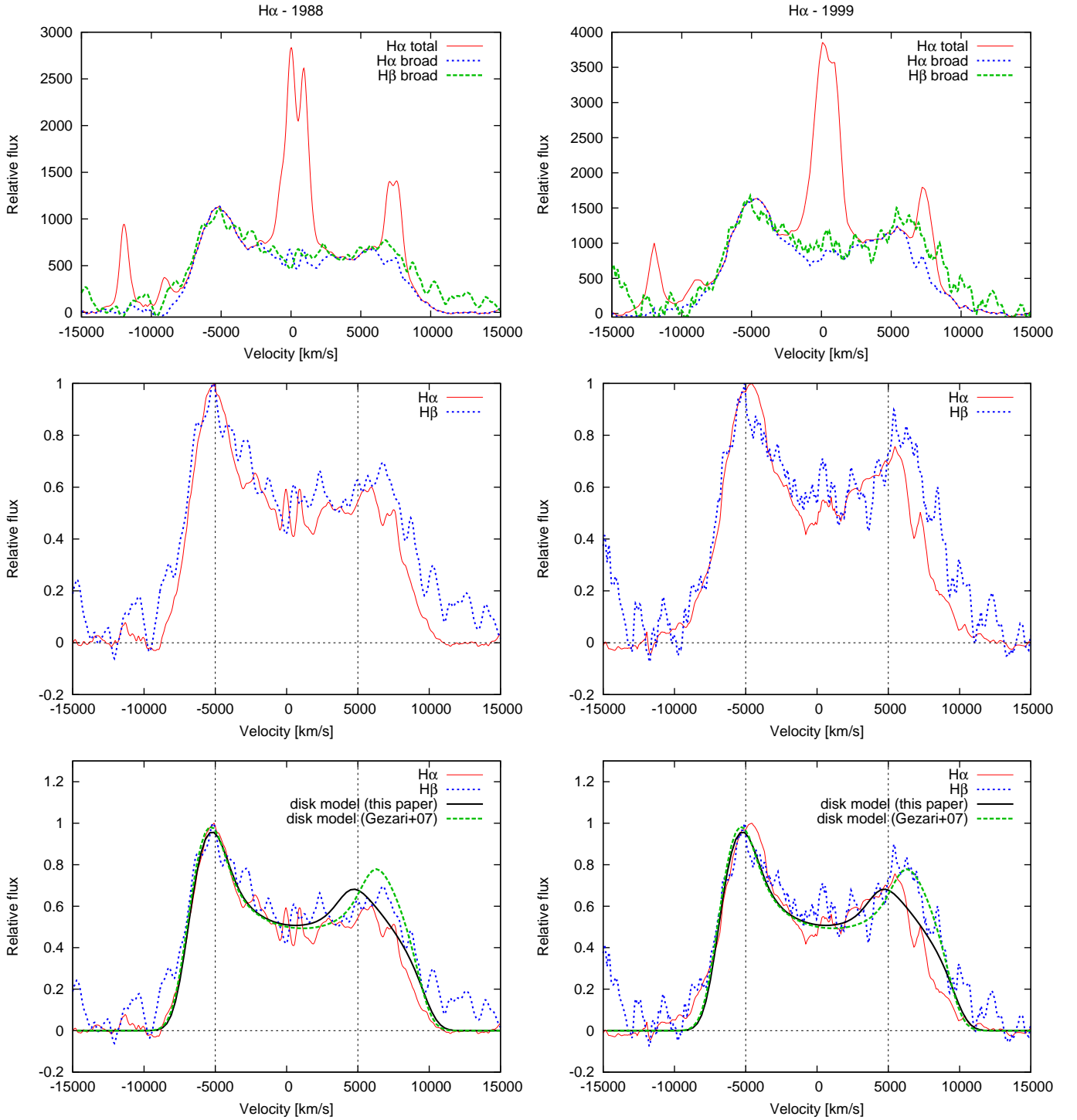


**Fig. 7.** The  $H\alpha$  line profiles in 1988 (left panels) and 1999 (right panels). Upper panels give total  $H\alpha$  line (with narrow lines) compared with broad  $H\alpha$  and  $H\beta$  component (multiplied with the constant to match the  $H\alpha$  blue peak), middle panels give normalized broad  $H\alpha$  and  $H\beta$  component, while bottom panels include disk models from this paper and Gezari et al. (2007).

### 3.1. Gaussian analysis - Changes in the broad line profiles

The parameters from the Gaussian fittings are given in Tables 2 and 3. As it can be seen from Tables, the  $H\alpha$  and  $H\beta$  blue peak positions are changing during the observed period for about  $\pm 500 \text{ km s}^{-1}$  around the averaged values (see Fig. 9 and Table 2), while the red-peak positions are changing for  $\pm \sim 1000 \text{ km s}^{-1}$  around averaged ones, that may also be due to the measurement uncertainties.

In general, the  $H\alpha$  profiles are of much better quality than  $H\beta$ , thus we plotted in Fig. 10 the results of the peak-measurements of the  $H\alpha$  line: the blue- vs. red-peak intensity (upper panel), and the blue- vs. red-peak velocity (down). It is interesting that there is no correlation between the velocities of the red and blue peaks (see Fig. 10, bottom panel), i.e. there may be a trend of an anticorrelation (but statistically not significant,  $r=-0.28$ ,  $P_0=0.08$ ), and it seems that they vary independently of

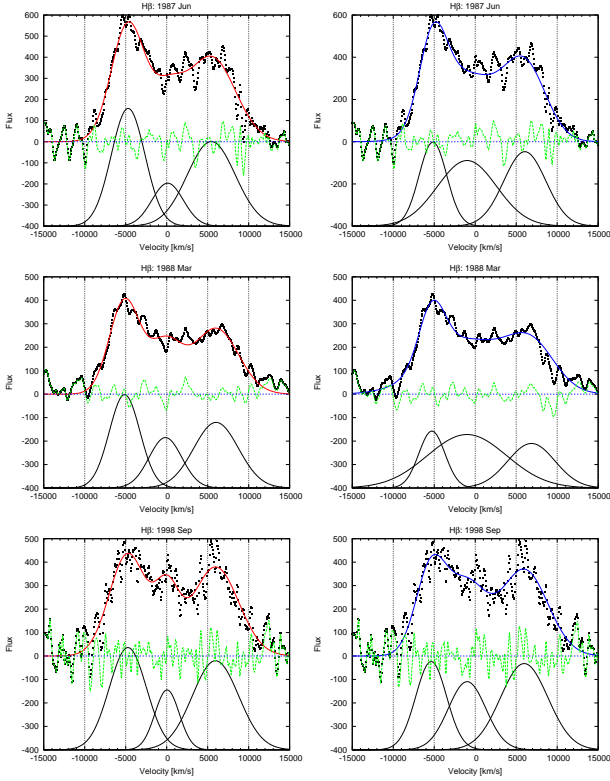


**Fig. 6.** The same as in Fig. 5 but for  $H\beta$  line.

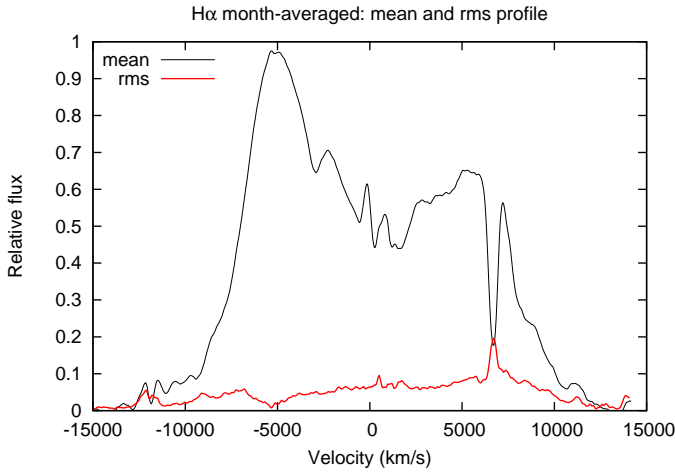


**Fig. 8.** The mean and rms of the  $H\alpha$  line profile obtained from the monthly-averaged profiles normalized to the intensity of the blue peak.

each other. But there is a good correlation between two peak intensities (see Fig. 10, upper panel) and the blue- and red-peak intensities are responding to each other.

In order to compare the position of the blue peak from our monitoring campaign with previous campaigns, we plot in Fig. 11 (upper panel) our measurements of the blue peak velocity for the  $H\alpha$  line together with the measurements of Newman et al. (1997) and Gezari et al. (2007). As it can be seen from Fig. 11, the agreement between different measurements is good, and differences are within the error-bars ( $\pm 100$ - $200 \text{ km s}^{-1}$ ). In Fig. 11 (bottom panel) we compared the blue- and red-peak positions between  $H\alpha$  and  $H\beta$  during monitored period. As it can be seen

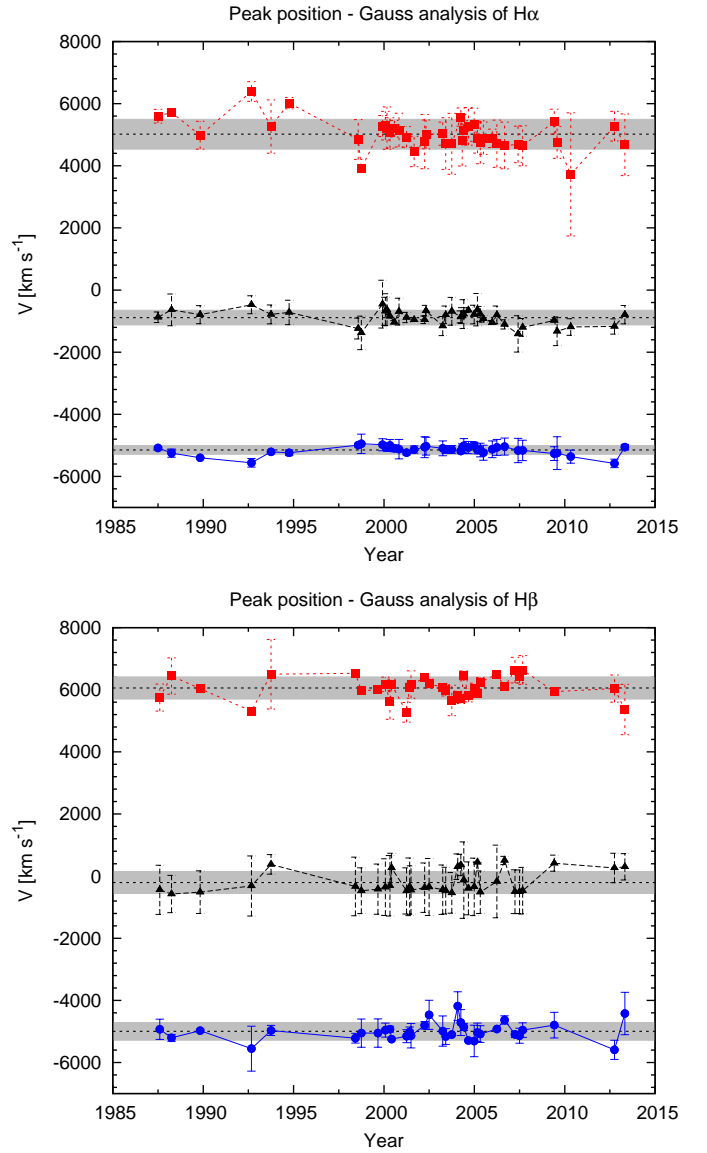


**Fig. 9.** The variability of the peak velocity obtained from the Gaussian fitting (red, central, blue) of  $H\alpha$  (upper) and  $H\beta$  line (bottom).

from Fig. 11 (bottom panel), there is a discrepancy between the positions of the red peaks of  $H\alpha$  and  $H\beta$  (in some periods for about  $2000 \text{ km s}^{-1}$ ), while the blue-peak position in both lines has no big change. There are small differences between the  $H\alpha$  and  $H\beta$  blue-peak positions, which are below  $\sim 500 \text{ km s}^{-1}$  (see also Tables 2 and 3).

In Fig. 12 we plot the  $H\alpha$  vs.  $H\beta$  peak velocity for the central (upper), blue (middle) and red (bottom) peak of Gaussians from the month-averaged profile fits. As it can be seen from Fig. 12 there are no expected correlations. However, it seems that a trend of anti-correlation is present in the red  $H\alpha$  vs.  $H\beta$  velocities (solid line on the plot), while a correlation trend may be present between the blue-peak velocities of  $H\alpha$  and  $H\beta$ . We should note that a trend of anti-correlation between the red-peak position may be caused by the measurement uncertainties, but that is not the case for the blue-peak positions. A theoretical expectation is that the velocity of the blue peak of the  $H\alpha$  line follows the one in the  $H\beta$  line, and, as can be seen in Fig.12 (middle) there



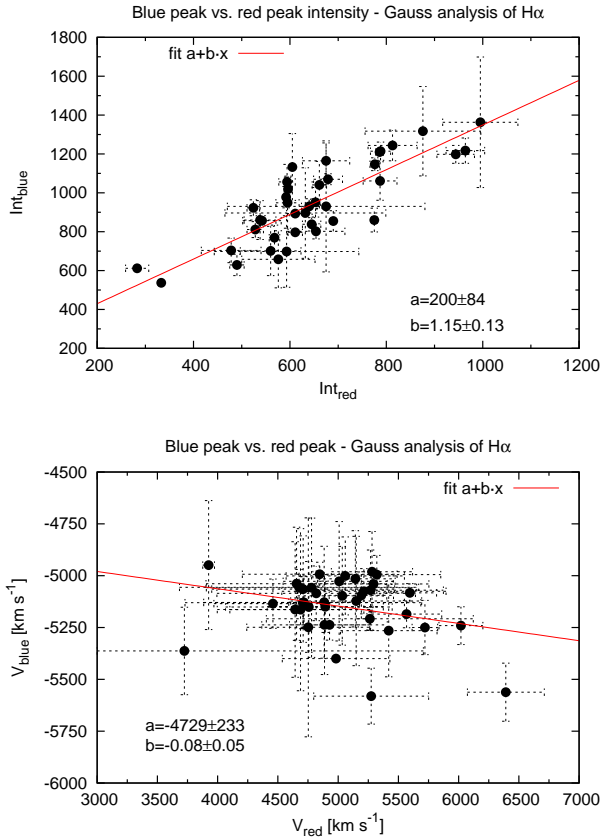


**Fig. 10.** The blue- to red-peak intensity (upper) and velocity (bottom) of H $\alpha$ . The correlation between the intensities is significant ( $r=0.83$  and  $P_0=0.5E-10$ ), while the anti-correlation between velocities is weak ( $r=-0.28$ ) and statistically is not significant ( $P_0=0.08$ ).

may be a slight dependence between the blue-peak velocities of H $\alpha$  and H $\beta$ , but it seems to be very weak (even taking into account the uncertainties in the measurements which are shown on the plots). This confirms that there are no expected correlations between the peak velocities of two broad lines.

### 3.2. Disc-model of the broad emission lines

As we noted above, the relativistic disc model (Chen et al., 1989; Chen & Halpern, 1989; Gezari et al., 2007) can explain the broad double-peaked profiles of Arp 102B. We performed several fits, and it was interesting that the month-averaged profiles can be successfully fitted with the simple Chen et al. (1989) disc model. The problem is that in some periods we could fit the line profiles only if we change the inclination of the disc for about 10 degrees, that is not expected. Note here that in the case when the inclination was fixed we obtain the satisfied fit by varying the other parameters (e.g. the emissivity and inner radius). Here we will not present all fits, only we present examples of the fits with parameters given by Gezari et al. (2007): the inner radius  $R_{\text{inn}} \sim 325 R_g$ , the outer radius  $R_{\text{out}} \sim 825 R_g$ , the disc inclination  $i \sim 31$  deg, the random velocity in the disc  $\sigma = 1050$  km s<sup>-1</sup>, with the emissivity  $r^{-q}$ , where  $q = 3.0$  is assumed (see Figs. 7 and 13). Additionally, starting from the parameters given above, we find the best fit of the mean H $\alpha$  profile, only changing the inclination taking  $i = 23$  deg, and that the line is blue-shifted at  $-900$  km s<sup>-1</sup>. As an example, two fits are com-

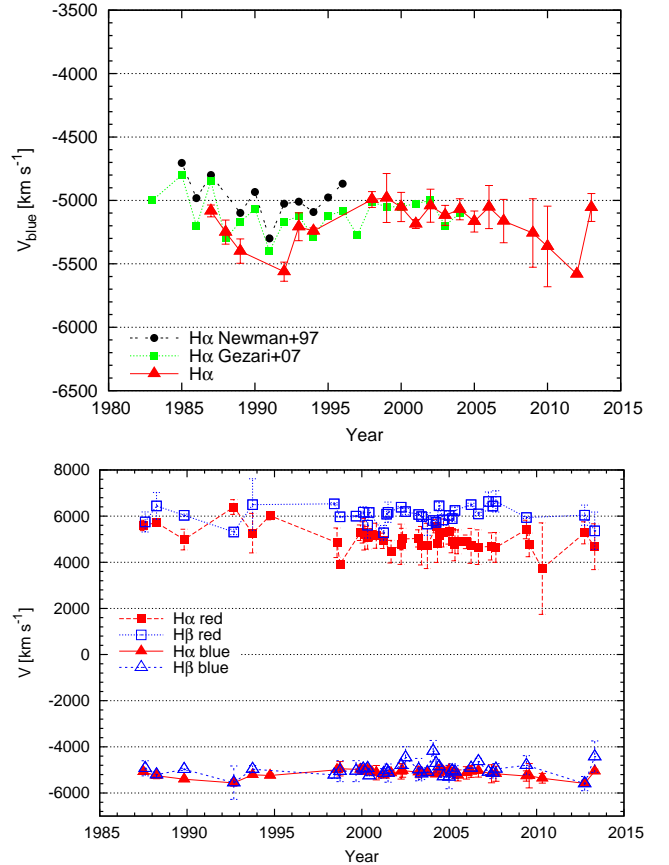


**Fig. 11.** Upper: Year-averaged radial velocities of the blue peak. The different symbols represent: full squares - the H $\alpha$  data from Gezari et al. (2007) year-averaged to match our data, full circles - the H $\alpha$  given in Newman et al. (1997) year-averaged to match our data, full triangles - our data for H $\alpha$ . Bottom: Month-averaged radial velocities of the blue and red peak positions for H $\alpha$  and H $\beta$ .

pared with observations from two periods for the H $\alpha$  and H $\beta$  line in Fig. 7 (bottom panel). As it can be seen in Fig. 7, the agreement with the blue peak of observations and both models are good, but differences are in the red wing. But we emphasize again that the narrow line subtraction may contribute to the uncertainty in the red-peak properties that can thus affect the obtained disc parameters.

If we consider the mean profile during the whole monitored period, one can conclude that the disc inclination is around  $i = 23$  deg, while the disc dimensions are around  $500 R_g$ . There is agreement between the disc parameters from our fit of the mean H $\alpha$  profile and one given in Gezari et al. (2007), apart from the disc inclination. However, by varying other parameters we were able to obtain  $i \sim 30$  deg, but in all fittings the disc dimensions seem to be very compact (about several 100s gravitational radii). In Fig. 13 we plotted both models together with the normalized mean H $\alpha$  profile.

As a conclusion, the line shape (double-peaked profiles) can be mainly fitted with a simple relativistic disc model, but the problem is, that, to fit the same line from different periods, one should change the disc parameters, as e.g. inclination or emissivity. This, in principle is not expected, but we should point out that the obtained parameters from the fit are strongly depending on the positions and intensities of the blue and red peaks, and

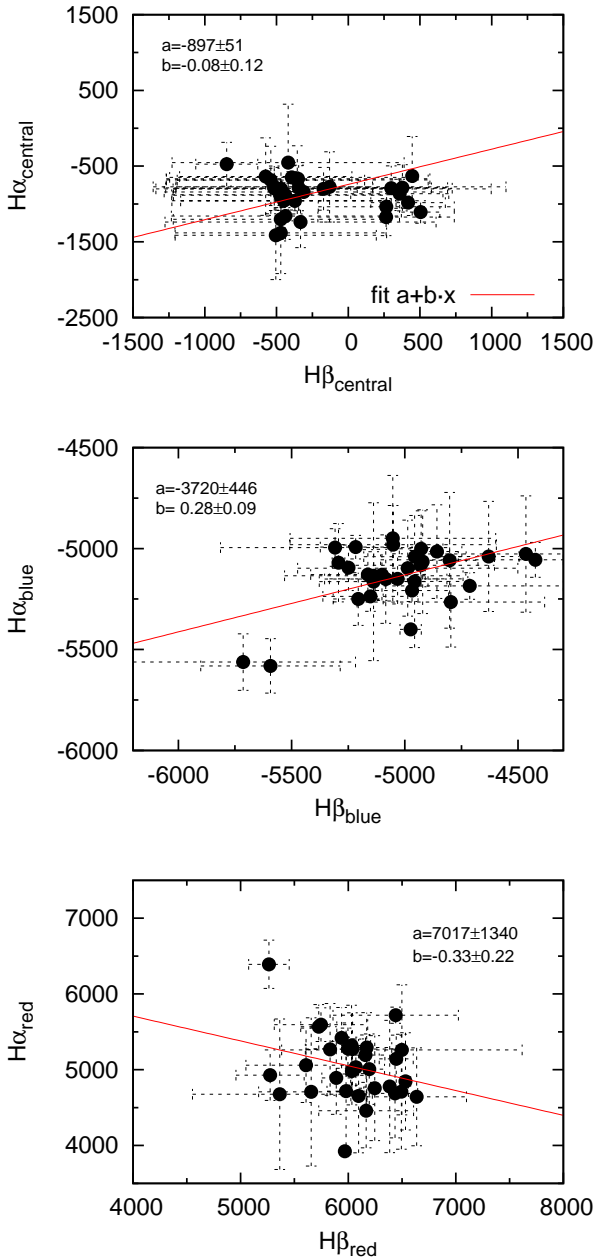


**Fig. 12.**  $H\alpha$  vs.  $H\beta$  peak velocity for the central (upper), blue (middle) and red (bottom) peak from the month-averaged profiles. The dashed line represents the expected function for an equal peak position in both lines, while solid line represents the best fit of the measured data. The correlation coefficients are:  $r=-0.12$  ( $P_0 = 0.5$ ) for the central,  $r=0.51$  ( $P_0=0.3E-02$ ) for the blue peak, and  $r = -0.26$  ( $P_0 = 0.15$ ) for the red peak. The parameters of the best fit are given on the plots.

as it was noted above there are relatively big uncertainties in the red-peak properties.

#### 4. Discussion

Double-peaked broad emission lines signature expected from the disc-like BLR, are observed in the spectrum of Arp 102B (Chen & Halpern, 1989; Eracleous & Halpern, 1994; Sergeev et al., 2000; Gezari et al., 2007; Shapovalova et al.,

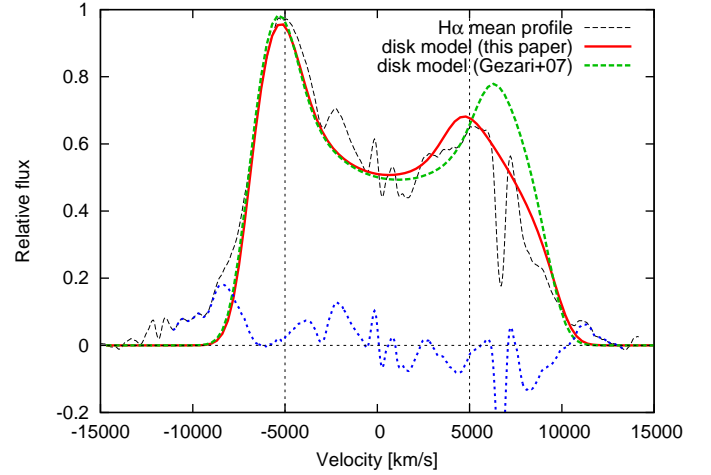


**Fig. 13.** The mean normalized  $H\alpha$  line profile fitted with the disc-model: solid line – our assumption (see text) and thick dashed line – parameters taken from Gezari et al. (2007). The residual at the bottom corresponds to the difference between the disc model from this paper and mean profile.

2013). The double-peaked lines are presented in a small fraction of AGNs (see Strateva et al., 2003). The double-peaked line profiles have been explained with a number of different models: a) binary black holes (see e.g. Gaskell, 1983), b) bipolar outflows (see e.g. Zheng et al., 1991), c) anisotropically illuminated spherical distribution of optically thick clouds (Goad & Wanders, 1996), d) circular or elliptical accretion disc (see e.g. Chen et al., 1989; Chen & Halpern, 1989; Eracleous et al., 1995, 1996), and e) other more sophisticated models like precessing elliptical disc or a circular disc with a long-lived, single-armed spiral or warp (see e.g. Gezari et al., 2007; Jovanović et al., 2010).

Here we can exclude the binary black hole (see e.g. Gaskell, 1983) model, since there is no significant changes in the position of the line peaks. Additionally, the model of anisotropically illuminated spherical distribution of optically thick clouds (Goad & Wanders, 1996) has a problem to explain a big distance between line peaks (more than  $10000 \text{ km s}^{-1}$ ), therefore here we will consider the disc-like geometry of the BLR and possibility of outflows in the BLR.

##### 4.0.1. The BLR disc emission: pro and contra

As we noted above, the disc emission has been usually assumed to model double-peaked profiles of Arp 102B, however some observational facts from monitoring of the broad lines are in contradictions with the disc model. Recall here some of them (see Miller & Peterson, 1990; Gezari et al., 2004, 2007):

- Flares in the broad-line flux, that can be seen also in our observations (see Paper I), but this can be expected if there are some transient processes in the disc (see e.g. Jovanović et al., 2010).
- Systematic variations in full width at quarter maximum reported in Gezari et al. (2004), that also may be explained in the disc structure variation.
- Periodic oscillation of the red-to-blue wing flux ratio observed by Newman et al. (1997) and Shapovalova et al. (2013), also can be caused by rotating structure in the disc.

- Intensity of the red peak is sometimes higher than the blue one (see Figs. 3 and 4), also can be explained by perturbations in the disc structure (see e.g. Jovanović et al., 2010; Popović et al., 2011), as well as with a model of precessing elliptical disc (Gezari et al., 2007).

As one can see, that some observed facts, mentioned above, can be explained by a more complex and non stable configuration of the accretion disc, i.e. that emissivity enhancements such as transient shocks induced by tidal perturbations could be present, and that the change in line profile can be reproduced by changing the inner and outer radii of the line-emitting portion of the disc.

However, there are some other observational facts, which are in disagreement with the disc model hypothesis:

a) A lack of (or slightly anti-) correlations of the blue-to-red intensity ratio with FWQM, as it is shown in Fig. 14. In principle, one can expect in the relativistic disc that the ratio between the blue and red peak should increase with increasing of the FWQM, since, there should be no change in the inclination, the intensive blue peak indicates that the inner radius is closer to the central black hole. This should result in more extensive (and less intensive) red part, that should contribute to the broader line measured at FWQM. I.e. the observed tendency in  $I_{blue}/I_{red}$  vs. FWQM should correlate, but it seems this has an opposite trend (see Fig. 14). However, Lewis et al. (2010) demonstrated that in the case of a model of the non-axisymmetric disc, in some cases the red-to-blue peak ratio increases as the width of the profile increases. Also, note here that some indication of such anti-correlation in other double peaked AGNs can be seen in Lewis et al. (2010). They showed plots of red-to-blue peak ratio as a function of time and from a quick inspection one can see a few cases where the changes do not follow the expectation that the FWQM is decreasing as the red-to-blue peak ratio increases (or the blue-to-red peak ratio decreases).

b) The distance between the position of the red and blue peak is different for the  $H\alpha$  ( $\sim 10500 \text{ km s}^{-1}$ ) and  $H\beta$  ( $\sim 12000 \text{ km s}^{-1}$ ), i.e. the  $H\beta$  shows larger distance for about  $1500 \text{ km s}^{-1}$ , that, in the frame of the disc hypothesis, should give that the line is closer to the central black hole, and consequently that relativistic effects are more observable in the  $H\beta$  line profile. But, as it can be seen in Figs. 3 and 4, the blue boosted peak is more intensive in  $H\alpha$ , almost during whole monitored period. On the other side, such huge distances between the peaks indicate a fast rotating disc, that is probably close to the black hole. From the rms profile (see Paper I, Fig. 11) one can see that the change in the line profile is also two-peaked, i.e. there is a change in the broad line profile in red and blue peak in both lines, where the variability in the blue wing is significantly bigger than in the red one. Note here, that there is one central peak (more intensive in the  $H\beta$  line) in the rms profile, that may be caused by a central component (also see Fig. 11 from Paper I).

c) Additionally, it is confusing that there is no big change in the  $H\alpha$  normalized line profile during this long monitored period (see Figs. 3 and 8), as well as in the displacement of the peaks. If the emission is originating in the disc, the disc emission is very stable during time, i.e. there is no big change in the disc which affect the emission. On the contrary, the different peak intensity ratio (e.g. in some periods red peak of  $H\beta$  is more intensive than the blue one) indicates that long living changes in the disc structure should be present (see e.g. Jovanović et al., 2010; Popović et al., 2011). These changes should affect a compact disc ( $\sim 500$  gravitational radii, that is several light days),

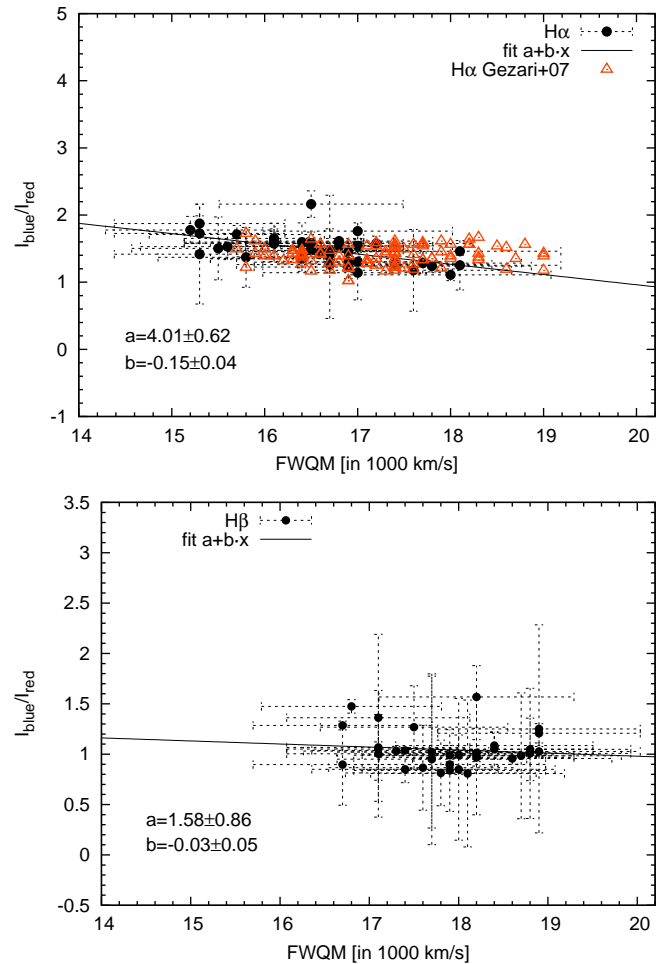


**Fig. 14.** The blue-to-red peak intensity ratio as a function of Full Width at Quarter of Maximum intensity (FWQM) for  $H\alpha$  (upper) and  $H\beta$  (bottom). The correlation coefficients are  $r = -0.55$  ( $P_0 = 0.2E-03$ ) and  $r = -0.14$  ( $P_0 = 0.4$ ) for  $H\alpha$  and  $H\beta$  respectively. The best fit parameters are given on the plots. The measurements for the  $H\alpha$  of Gezari et al. (2007) are given on upper plot (open triangles).

and consequently a stronger variability in the broad line profiles is expected.

d) Finally, the spectropolarimetric observations are also in contradictions with the BLR disc model. Spectropolarimetric observations (see Antonucci et al., 1996; Corbett et al., 1998, 2000) did not confirm the disc-like structure of the BLR in Arp 102B. Especially it is interesting that the angle of the jet direction ( $\sim 105$  degrees) corresponds to the polarization angle in the  $H\alpha$  line ( $\sim 103$  degrees, see Corbett et al., 1998). The  $H\alpha$  polarized shape of Arp 102B indicates a line-emitting biconical outflow surrounded by a cylindrical scattering region (Corbett et al., 1998, 2000). However, note here two facts which do not exclude disc model. First, that Chen et al. (1997) obtained a qualitative agreement between the disc model, but other possible explanations of the broad line polarization properties of Arp 102B are possible, as e.g. that to the disc emission there is additional outflow emission (see Fig. 15). Second, as it was mentioned in Afanasiev et al. (2014), the role of the inter-stellar polarization in the polarization properties of the broad lines is very important and after taking it into account, the polarization angle may be changed.

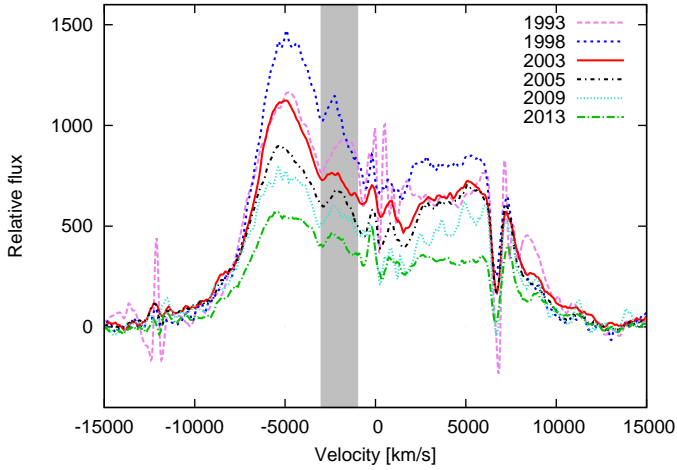


**Fig. 15.** Bump in the  $H\alpha$  line profile at  $\sim 2000\text{km s}^{-1}$  in years when it is most intensive.

#### 4.0.2. Outflow(s) in the Arp 102B BLR

Recently, Couto et al. (2013) found two-armed nuclear spiral (see also Fathi et al., 2011) in an extensive field around the nucleus of Arp 102B ( $2.5 \times 1.7 \text{ kpc}^2$ ) and they estimated that the mass outflow rate along one (the east) arm is between  $0.26\text{--}0.32 \text{ M}\odot\text{yr}^{-1}$ , that is higher than the mass accretion rate. Therefore, one can expect that an outflow is present in the BLR. As it can be seen in Fig. 15, during some periods, there is a bump in the blue part of the  $H\alpha$  line (around  $-2500 \text{ km s}^{-1}$ ), that may indicate that additionally to the disc emission, there is an outflow in the BLR.

In principle, a biconical outflow model can explain double-peaked line profiles (as e.g. Balmer line profiles of 3C 390.3, see Zheng et al., 1991). The blue-shifted and red-shifted peaks are produced by the approaching and receding parts, respectively. Additionally, a model where an accelerating outflow together with an inflow of the emitting gas is dominating in the BLR can explain very complex line profiles (also double-peaked Ilić et al., 2010; León-Tavares et al., 2014).

Also, spectropolarimetric observations seem to be in favor of the some type of a bi-conical model (see Corbett et al., 1998, 2000, and corresponding scheme).

As a summary, one can note that the outflow is probably present in the BLR, seen as a blue bump between the center of the line and blue peak (around  $-2500 \text{ km s}^{-1}$ , see Fig. 15), but it is not clear if the emission from the outflow is dominant in the broad line profiles. Also, one possible problem are relatively small changes in the broad line profiles, that, probably in the case of outflows should be higher.

## 5. Conclusion

We analyzed the variability in the broad line properties in a long period of 26 years of Arp 102B, an AGN with prominent double-peaked broad line profiles. We investigated the broad line profile variations during this period and from our investigations we can outline the following conclusions:

a) The broad line profiles have not been significantly changed in a period of 26 years in sense that during monitored time, the shift of peaks stays almost unchanged and there are flare-like changes in the line intensity, and some time in the ratio of the blue-to-red peak intensity. This is unusual if there is an

emission of relatively compact accretion disc (dimension smaller than  $1000 R_g$ ), since, changes in the intensity ratio of peaks should result in the line widths as well as in the displacement of the peak velocities. Moreover, the intensity ratio of peaks shows a trend of an anticorrelation with the line width, that is opposite what one can expect from the disc emission. Sometimes, the position of the red peak does not match the AD-model predictions (Fig. 6).

b) As an additional conclusion to our earlier one that the variation of fluxes of  $H\beta$  vs.  $H\alpha$  has a small correlation (see Shapovalova et al., 2013), there is practically no correlation between velocities of the blue and red peaks between the  $H\beta$  and  $H\alpha$  line. Moreover, the line profiles of  $H\beta$  and  $H\alpha$  are different,  $H\alpha$  has more intensive blue peak, and  $H\beta$  has almost equivalent intensity of peaks in the most of observations. Also, it is unexpected that the  $H\beta$  is significantly broader ( $\sim 1500 \text{ km s}^{-1}$ ) than  $H\alpha$ , and that the relativistic effect of the blue-boosting is more prominent in the case of  $H\alpha$

c) An outflow in the BLR seems to be present (from time to time it can be noticed as the blue bump around  $-2500 \text{ km s}^{-1}$ ). Although it is not clear how much the outflow can contribute to the broad line emission, it should be taken into account.

At the end, let us conclude that profiles of the broad double-peaked lines in Arp 102B can be fitted very well with the disc model, but there are several issues in the variation of the broad spectral line properties which are not in agreement with ones expected in the variability of the accretion disc structure. The better spectro-polarimetric observations/monitoring of Arp 102B are needed to study the polarization properties of the ordinary broad-line component in order to clarify of the BLR nature.

## Acknowledgments

This work was supported by INTAS (grant N96-0328), RFBR (grants N97-02-17625 N00-02-16272, N03-02-17123, 06-02-16843, N09-02-01136, 12-02-00857a, 12-02-01237a), CONACYT research grants 39560, 54480, and 151494 (Mexico), PROMEP/103.5/08/4722 grant, the Ministry of Education and Science of Republic of Serbia through the project Astrophysical Spectroscopy of Extragalactic Objects (176001), and DFG grant Ko 857/32-1. L. Č. P., W. K. and D. I. are grateful to the Alexander von Humboldt foundation for support in the frame of program "Research Group Linkage". We would like to thank the anonymous referee for very useful comments.

## References

- Afanasyev, V. L., Popović, L. Č., Shapovalova, A. I., Borisov, N. V., Ilić, D. 2014, MNRAS, 440, 519
- Antonucci, R., Hurt, T., Agol, E. 1996, ApJ, 456, L20
- Chen, K. & Halpern, J. 1989, ApJ, 344, 115
- Chen, K. Halpern, J. P., Filippenko, A. V. 1989, ApJ, 339, 742
- Chen, K., Halpern, J. P., Titarchuk, L. G. 1997, ApJ, 483, 194
- Corbett, E. A., Robinson, A., Axon, D. J., Young, S. 2000, MNRAS, 319, 685
- Corbett, E. A., Robinson, A., Axon, D. J., Young, S., Hough, J. H. 1998, MNRAS, 296, 721
- Couto, G. S., Storchi-Bergmann, T., Axon, D. J., Robinson, A., Kharb, P., Riffel, R. A. 2013, MNRAS, 435, 2982.
- Dimitrijević, M. S., Popović, L. Č., Kovačević, J., Dačić, M., Ilić, D. 2007, MNRAS, 374, 1181
- Eracleous, M., & Halpern, J. P. 1994, ApJS, 90, 1
- Eracleous, M., Halpern, J., Gilbert, A., Newman, J. A., Filippenko, A.V. 1997, ApJ, 490, 216
- Eracleous, M., Livio, M., Halpern, J.P., & Storchi-Bergmann, T. 1995, ApJ, 438, 610
- Eracleous, M., Halpern, J.P., & Livio, M. 1996, ApJ, 459, 89

- Fathi, K., Axon, D. J., Storchi-Bergmann, T., Kharb, P., Robinson, A., Marconi, A., Maciejewski, W., Capetti, A. 2011, *ApJ*, 736, 77
- Gaskell, C. M. 1983, *Liege International Astrophysical Colloquia*, 24, 473
- Gezari, S., Halpern, J. P., & Eracleous, M. 2007, *ApJS*, 169, 167
- Gezari, S., Halpern, J. P., Eracleous, M., Filippenko, A. V. 2004, *IAUS*, 222, 95
- Goad, M., & Wanders, I. 1996, *ApJ*, 469, 113
- Halpern, J. P., Eracleous, M., Filippenko, A. V., & Chen, K. 1996, *ApJ*, 464, 704
- Ilić, D., Popović, L. Č., Shapovalova, A. I., Kovačević, A., León-Tavares, J., Chavushyan, V. H. 2010, *Mem. Soc. Ast. It. Supp.*, 15, 166
- Jovanović, P., Popović, L. Č., Stalevski, M., Shapovalova, A. I. 2010, *ApJ*, 718, 168
- León-Tavares, J., Popović, L. Č., Ilić, D., Chavushyan, V. H. 2014, in preparation
- Lewis, K. T., Eracleous, M., Storchi-Bergmann, T. 2010, *ApJS*, 187, 416
- Miller, J. S., Peterson, B. M. 1990, *ApJ*, 361, 98
- Newman, J. A., Eracleous, M., Filippenko, A. V., Halpern, J. 1997, *ApJ*, 485, 570
- Popović, L. Č., Mediavilla, E., Bon, E., & Ilić, D. 2004 *A&A* 423, 909
- Popović, L. Č., Mediavilla, E. G., Muñoz, J. A. 2001, *A&A*, 378, 295
- Popović, L. Č., Shapovalova, A. I., Ilić, D., Kovačević, A., Kollatschny, W., Burenkov, A. N., Chavushyan, V. H., Bochkarev, N. G., León-Tavares, J. 2011, *A&A*, 528A, 130
- Riffel, R., Rodríguez-Ardila, A., & Pastoriza, M. G. 2006, *A&A*, 457, 61
- Shapovalova, A. I., Popović, L. Č., Burenkov, A. N., et al. 2013, *A&A*, 559, A10
- Sergeev, S. G., Pronik, V. I., Sergeeva, E. A. 2000, *A&A*, 356, 41
- Strateva, I. V., Strauss, M. A., Hao, L., et al. 2003, *AJ*, 126, 1720
- Sulentic, J. W., Zheng, W., Calvani, M., Marziani, P. 1990, *ApJ*, 355, 15
- Zheng, W., Veilleux, S., Grandi, S. A. 1991, *ApJ*, 381, 418.

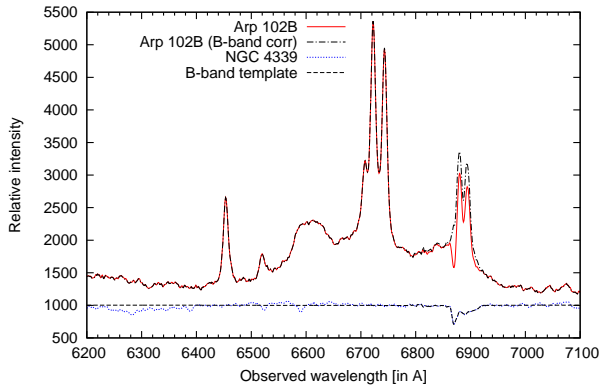


**Fig. A.1.** The correction of the  $H\alpha$  line on B-band absorption. The spectrum of NGC 4399 (shown below) is observed in the same epoch (Mar 26, 2003) as the spectra of Arp 102B.

## Appendix A: The line fitting procedure and narrow line subtraction

One of the problems in the measurements of the broad line parameters is the uncertainty in the narrow line subtraction, especially in the red peak of  $H\alpha$  and  $H\beta$ , since the narrow lines are right on top of the red peak in both broad lines. Therefore, to find uncertainties of the narrow line subtraction we did several tests. Additionally, we consider the B-band absorption observed near the [SII] doublet in the  $H\alpha$  wavelength range.

### A.1. Correction of the B-band absorption near [SII]

The B-band absorption is present in the red wing of the  $H\alpha$  line, near the narrow [SII] doublet (see Fig. A.1). To correct this absorption we used the template spectrum of NGC 4339, which was observed at the same night as Arp 102B with 2.1m GHO telescope with resolution  $\sim 8\text{-}9 \text{ \AA}$  on Mar 26, 2003. Then we corrected the B-band absorption near the [SII] lines in the  $H\alpha$  spectral region.

In Fig. A.1 we illustrate the correction of the B-band absorption. As one can see in Fig. A.1 the absorption is well corrected, but in some spectra the residuals are still present. However, the residuals are weak and can not affect the narrow line estimates, as well as the estimates of the red-peak position in  $H\alpha$  (see following section and Figs. A.2). Therefore, we accepted the parameters from the fits where the B-band absorption was not corrected.

### A.2. Estimation of the narrow line emission

As we mentioned above, the uncertainties in the estimations of the broad line parameters come mainly from the subtraction of the narrow lines in the  $H\beta$  and  $H\alpha$  spectral range. It is hard to handle the removal of the narrow emission lines in Arp 102B, because the narrow lines are right on top of the red peak in the  $H\alpha$  and  $H\beta$  broad lines. To explore the uncertainty in the narrow line subtractions we performed two approaches: i) fitting the narrow lines with Gaussian functions before and after the B-band absorption has been corrected (as described in §2.2), and ii) estimation of the broad profile using spline fitting (using DIPSO). In Figs. A.2 and A.3 we illustrated the subtraction of the narrow lines using these two methods. In Fig. A.2 (fourth panel) we compared the broad  $H\alpha$  line profile obtained after the subtraction of the narrow lines using these two procedures (note that we

fitted the spectra before and after the correction for the B-band absorption). As it can be seen in Fig. A.3 (bottom panel), the fitted position of the blue and red peaks is practically the same also for  $H\beta$  for both procedures, therefore we used the Gaussian decomposition in our estimates of the narrow line contribution.

### A.3. Correction of the fits using the ratio of the narrow lines

As we mentioned above, some parameters of the narrow lines are fixed in the spectral fit; first of all the Gaussian velocity dispersions and shift for all narrow lines in the line wavelength range, as well as the ratio of the [OIII]4959,5007, that is fixed to 1:3 (Dimitrijević et al., 2007). Also, one cannot expect that the ratio of narrow lines is changing during the period of several years. Therefore one very clear way to test the robustness of the narrow line fittings is to compute the emission line ratios for each combined fit.

The timescale of the observations is long enough that there could be some variation in the narrow emission line ratios, but certainly over timescales of  $\sim 5\text{-}10$  years there should not be major changes in the narrow line ratios (except of the random scatter). We calculated the narrow line ratios of [NII]/ $H\alpha$ , [OI]6300/ $H\alpha$ , [SII]6715/ $H\alpha$ , and [OIII]5007/ $H\beta$ . The line ratios in the  $H\alpha$  and  $H\beta$  wavelength range are presented in Fig. A.4, where dashed lines represent the averaged ratio and shaded regions the  $\pm 10\%$  of the averaged value. As it can be seen in the upper panels of Fig. A.4, there is not any trend in the line ratio variability during the monitored period. Consequently, we corrected those fits for which the narrow line ratios were significantly different from the mean value, i.e. the spectra with a big narrow line ratio difference have been re-fitted taking the constraint in the fit that the line ratio has to be in the frame of  $\pm 15\%$  of the corresponding mean value. In Fig. A.4, bottom panels, the line ratios are shown after the correction of a number of spectra.

### A.4. The broad line fit and estimates of the parameter uncertainties

To find the broad line parameters of the  $H\alpha$  and  $H\beta$  broad lines, we performed the Gaussian analysis, fitting the month-averaged broad line profiles. The broad profile was fitted with three Gaussian functions, corresponding to the blue, central, and red component (Fig. 5). Each Gaussian was described with three free parameters, i.e. in the fit procedure we have nine free parameters: three intensities, widths and shifts of Gaussian functions which describe the blue, central and red part of the broad line.

Inspection of the obtained parameters from the fit, as well as several additional tests (changing slightly parameters), showed that the central component, is often shifted to the blue (especially in  $H\alpha$ ) and that, in some cases, this component has a big (unexpected) change in the shift. Additionally, we found that the position of the central component can significantly affect parameters of the peaks, especially the red one. Therefore, we repeated the fitting procedure with three broad Gaussian functions, but putting the limits on the shift of the central component to be between  $-1000 \text{ km s}^{-1}$  and  $600 \text{ km s}^{-1}$ . Using this procedure we obtained an additional set of broad line parameters (parameters of the blue, central and red Gaussians). Inspection of differences between the parameters obtained from the fits with and without constraint of the central component shift showed that the peak positions are not significantly changed, but the intensities of the

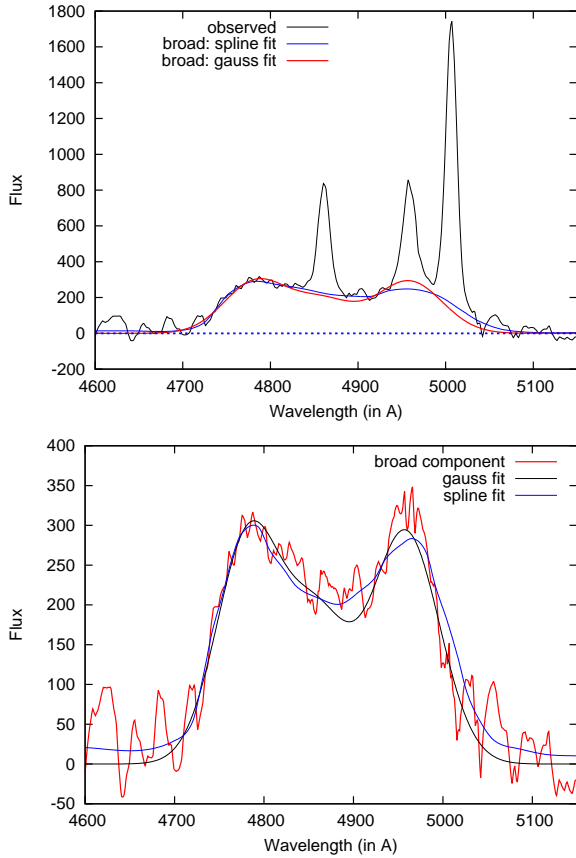


**Fig. A.3.** Upper panel: Narrow lines removed in  $H\beta$  using the DIPSO spline fitting of the broad component, compared with the 3-gaussian broad-component fitting. Bottom panel: Comparison of the  $H\beta$  broad component (after narrow lines subtraction) using the 3-gaussian and DIPSO spline fitting. The blue peak position is the same, a slight difference is seen in the red one.

red peak, the shift of the central component, and the widths of the components have been significantly changed.

We compared the error-bars from the fits with differences between the parameters from these two fitting procedures, and found that the error-bars of parameters are often significantly smaller than the differences between the parameters from both fits. Therefore, we calculated the averaged parameters from the two fits, and accepted uncertainties (error-bars) as discrepancy between the parameters from the two fits. The averaged broad line parameters and corresponding estimated uncertainties are given in Tables 2 (for  $H\alpha$ ) and 3 (for  $H\beta$ ).

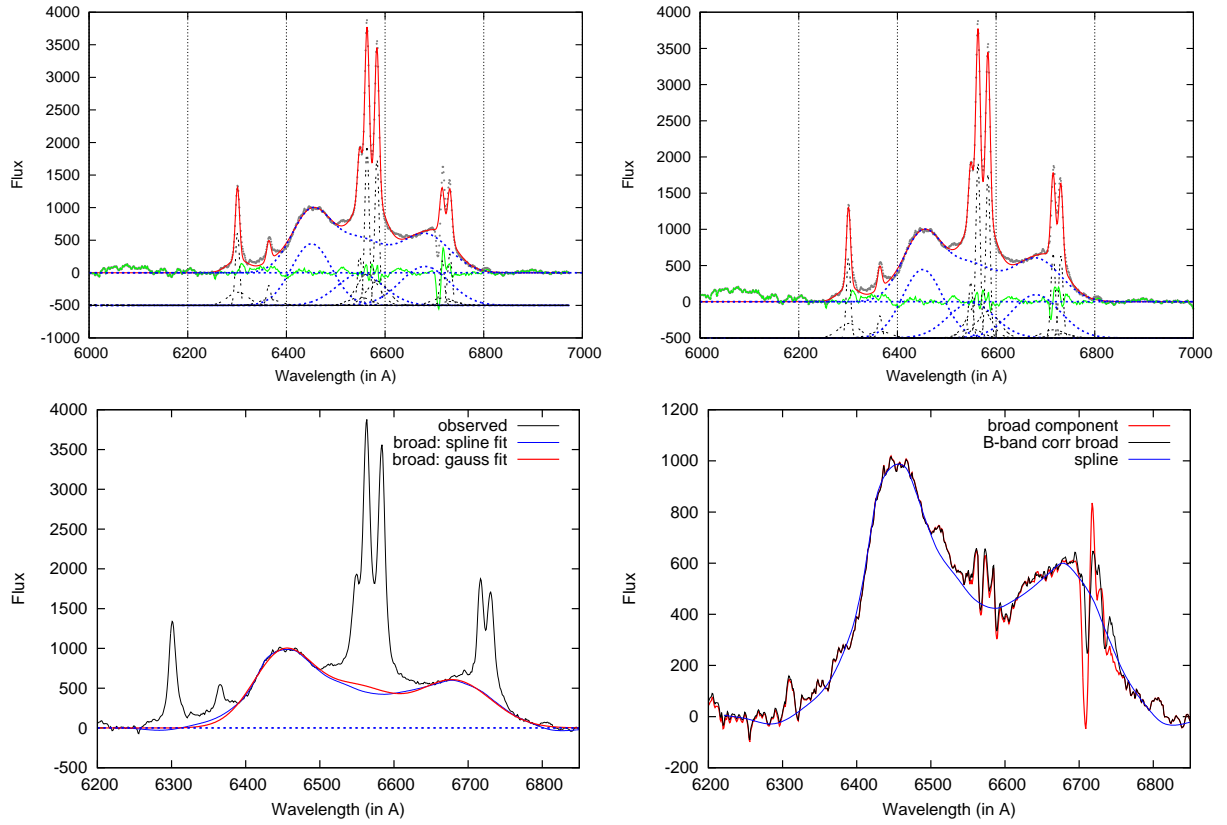


**Fig. A.2.** Multi-gaussian fitting of the  $H\alpha$  wavelength range of the spectrum observed on Apr 02, 2003. Upper left: Fitting of the spectra where the B-band absorption is not corrected. Upper right: The same but for the B-band corrected observed spectrum. In these two plots same Gaussians parameters (apart for the [SII] lines which intensities are only increased) have been used. Bottom left: Narrow lines removed using the DIPS0 spline fitting of the broad component, compared with the 3-gaussian broad-component fitting. Bottom right: Comparison of the  $H\alpha$  broad component (after narrow lines subtraction) before and after the B-band absorption correction and the broad component obtained using the DIPS0 spline fitting. The blue peak position is the same, a slight difference is seen in the red one.



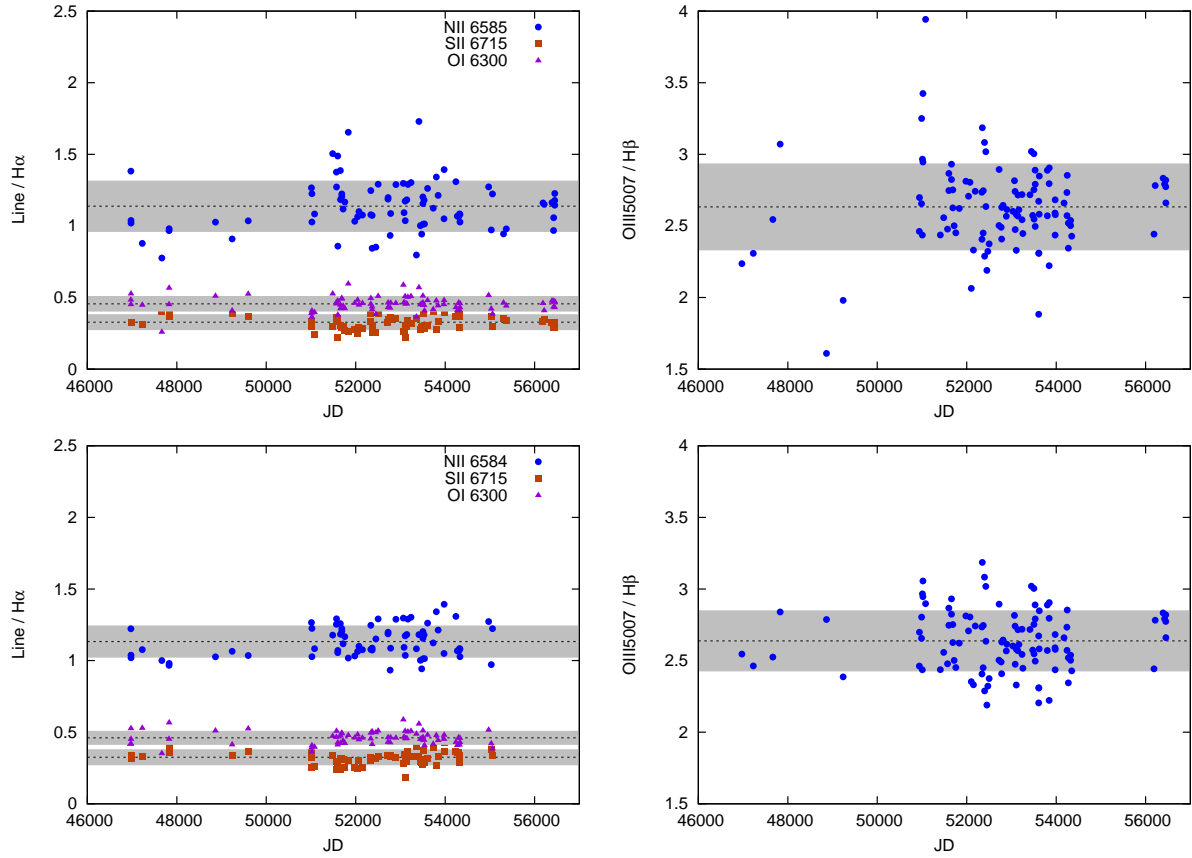


**Fig. A.4.** The ratio of the narrow emission line (labeled on plots) fluxes (in the  $H\alpha$  and  $H\beta$  wavelength range) during the monitored period. The narrow lines fluxes are calculated from the Gaussian fitting parameters as a sum of two components (one narrower fitting the line core and one broader fitting the line wings, see §2.2) The dashed lines with the shaded regions represent the mean value and the deviation of 10% from this. On upper panels, the ratios obtained from the fit without any constraint, while in the bottom panels, the points with big scattering (from panel up) have been corrected.